



Microstructurally validated stable and predictable swelling in low-enriched uranium monolithic U-10Mo fuel mini-plates

May 2025

Changing the World's Energy Future

William Alexander Hanson, Daniele Salvato, Adam B Robinson, Nancy J Lybeck, Jan-Fong Jue, Tammy L Trowbridge, Jatuporn Burns, Fidelma G. Di Lemma, Charlyne A. Smith, Margaret A Marshall, Dennis D. Keiser Jr., Jeffrey J Giglio, James I. Cole



DISCLAIMER

This information was prepared as an account of work sponsored by an agency of the U.S. Government. Neither the U.S. Government nor any agency thereof, nor any of their employees, makes any warranty, expressed or implied, or assumes any legal liability or responsibility for the accuracy, completeness, or usefulness, of any information, apparatus, product, or process disclosed, or represents that its use would not infringe privately owned rights. References herein to any specific commercial product, process, or service by trade name, trade mark, manufacturer, or otherwise, does not necessarily constitute or imply its endorsement, recommendation, or favoring by the U.S. Government or any agency thereof. The views and opinions of authors expressed herein do not necessarily state or reflect those of the U.S. Government or any agency thereof.

Microstructurally validated stable and predictable swelling in low-enriched uranium monolithic U-10Mo fuel mini-plates

William Alexander Hanson, Daniele Salvato, Adam B Robinson, Nancy J Lybeck, Jan-Fong Jue, Tammy L Trowbridge, Jatuporn Burns, Fidelma G. Di Lemma, Charlyne A. Smith, Margaret A Marshall, Dennis D. Keiser Jr., Jeffrey J Giglio, James I. Cole

May 2025

**Idaho National Laboratory
Idaho Falls, Idaho 83415**

<http://www.inl.gov>

**Prepared for the
U.S. Department of Energy
Under DOE Idaho Operations Office
Contract DE-AC07-05ID14517**

Microstructurally Validated Stable and Predictable Swelling in Low-Enriched Uranium Monolithic U-10Mo Fuel Mini-Plates

William A. Hanson^{1*}, Daniele Salvato¹, Adam B. Robinson¹, Nancy J. Lybeck¹, Jan-Fong Jue¹, Tammy L. Trowbridge¹, Jatuporn Burns¹, Fidelma G. Di Lemma¹, Charlyne A. Smith¹, Margaret A. Marshall¹, Dennis D. Keiser Jr.¹, Jeffrey J. Giglio¹, James I. Cole¹

1. Idaho National Laboratory, P. O. Box 1625, Idaho Falls, ID 83415-6188 U.S.A.

*Corresponding Author: William.Hanson@inl.gov

Abstract

Qualification of the low-enriched uranium (LEU) monolithic U-10wt%Mo (U-10Mo) plate-type fuel system requires a demonstration of a stable and predictable fuel swelling behavior over the anticipated operating conditions of the United States high-performance research reactors (USHPRRs) selected for conversion to LEU operation. This will allow each reactor to develop appropriate safety margins that will retain fuel element lifetime coolability. Additionally, the fuel system must maintain performance attributes when fabricated at a commercial scale. The Mini-plate 1 experiment represents the first irradiation test of commercially fabricated miniaturized monolithic LEU U-10Mo fuel plates. The swelling behavior within this experiment was compared against that of historical fuel developmental tests to reveal that the commercially fabricated fuel performed within the current recommended U-10Mo swelling model's predictions. Additionally, the fuel microstructural evolution was evaluated to link initial conditions to subtle variations detected in the swelling response, providing validation and confidence that the fuel system is robust.

1. Introduction

In memoriam of Dr. Dennis D. Keiser Jr.

Five United States high-performance research reactors (USHPRRs) and one associated critical facility are targeted for conversion to Low Enriched Uranium (LEU) operation, where ²³⁵U enrichment is <20%. A new high U-density LEU plate-type fuel must be qualified to retain the current operational mission for the USHPRRs. Through years of developmental experiments, an Al-alloy clad, monolithic U10wt%Mo (U-10Mo) fuel with Zr diffusion barrier was selected as the first new LEU fuel to be qualified to begin converting these USHPRRs [1, 2]. To be qualified, the new fuel system must be demonstrated to maintain mechanical integrity, geometric stability, and operate stably and predictably over the operational envelope of the converting reactors. Additionally, the fuel system must be economically fabricable at scale, and the Mini-Plate 1 (MP-1) experiment represents the first irradiation campaign in this qualification program to irradiate commercially fabricated miniaturized (mini) plates [3, 4].

A more extensive analysis of the design of the MP-1 experiment was published separately by S.M. Kilby et al. [4], so only a brief overview will be provided here. MP-1 consisted of 74 Al-alloy 6061 clad mini-plates (nominally 101.47 × 25.4 × 1.24 mm) containing a monolithic U-10Mo foil fuel core with a hot-roll bonded Zr diffusion barrier, nominally 25.4 μm thick on each side. Two fuel thicknesses were included, with thicker fuel foils designed for irradiation at low power (LP) density and thinner fuel foils

designed for irradiation at medium power (MP) density. To provide a baseline reference to the historical fabrication, 12 of the mini-plates (8 LP and 4 MP) were fabricated at the Idaho National Laboratory (INL), referred to as “B-plates”, while the balance of mini-plates was fabricated by a commercial vendor, referred to as “C-plates”. While there are several subtle differences between the baseline and commercial fabrications, most of which involve proprietary processes, the main thermal treatment distinction in the latter was the inclusion of a homogenization anneal of the as-received fuel feedstock coupons [3], which was absent in the baseline mini-plate fabrication. Unirradiated characterization of archived mini-plates demonstrated this anneal homogenized the Mo-content of the fuel foils in the MP-1 C-plates [5]. A summary of the MP-1 plate types is included in Table 1.

Table 1 – Summary of MP-1 plate-types and irradiation conditions [4, 6, 7, 8, 9]

	<i>LP Thick Fuel</i>	<i>MP Thin Fuel</i>
<i>Nominal Fuel Foil Thickness</i>	0.6350 mm	0.2159 mm
<i>C-plates (with homogenization)</i>	34	28
<i>B-plates (without homogenization)</i>	8	4
<i>Total Plates</i>	42	32
<i>ATR Irradiation Position</i>	B-position	South Flux Trap
<i>Average Peak Power Density</i>	5–10 kW/cm ³	20–35 kW/cm ³
<i>End of Life Fission Density</i>	0.63–3.15×10 ²¹ fissions/cm ³	2.52–6.11×10 ²¹ fissions/cm ³

A thorough understanding of the fuel swelling phenomena in the U-10Mo fuel system is vital to demonstrating the fuel design is geometrically stable and predictable under the operating conditions proposed for qualification [1, 2]. Recently, Robinson et al. published an extensive analysis developing an empirical U-10Mo swelling model, based on the historic irradiation experiments. This model is currently recommended by the USHPRR program Fuel Qualification (FQ) pillar as a conservative estimate of swelling as a function of fission density [1, 10]. As the MP-1 experiment is the first U-10Mo irradiation test following this effort, of particular interest is defining the swelling behavior of each mini-plate in the experiment and comparing it against this model. This is both a test of the efficacy of the model at predicting a new irradiated U-10Mo fuel dataset and an evaluation of the MP-1 swelling behavior in context of the historical performance.

2. Materials and Methods

2.1 Irradiation conditions

A substantially more detailed discussion of the MP-1 experiment irradiation conditions, as well as the experimental validation of the as-run neutronics modelling, is being published separately by M.A. Marshall et al., so this work will only provide a summary overview of each for brevity. The MP-1 experiment was irradiated in the Advanced Test Reactor in a combination of “B” positions for the LP thick fuel plates and the south flux trap for MP thin fuel plates. The irradiation portion of the MP-1 experiment was concluded early after the cladding bond-line separation of two LP B-plates; however, the root cause analysis of the bond-line separation is not the subject of this study [11, 12]. The final irradiation condition bounds for MP-1 are listed in Table 1 [6, 7, 8, 9].

2.2 Overview of Post-Irradiation Examinations

Following irradiation at the ATR, a suite of non-destructive and destructive examinations (NDE & DE, respectively) were conducted on the MP-1 test trains at the Materials and Fuels Complex (MFC) Hot Fuel Examination Facility (HFEF). A summary of each of the individual post-irradiation examinations (PIE) performed will be provided in the forthcoming M.A. Marshall et al. publication; however, the

techniques pertinent to the analysis presented in this work will be overviewed, specifically PIE plate profilometry and destructive sectioning. The PIE plate thickness of each MP-1 mini-plate was measured on a 1×2 mm measurement grid, using the BONA4INL Measurement Bench, which has a thickness and location resolution of $\pm 3 \mu\text{m}$ and $\pm 20 \mu\text{m}$, respectively [13]. After each plate thickness profilometry measurement, the oxide thickness was measured via eddy current contact probes over the same measurement grid. Following NDE, plates of each fabrication were strategically selected from different test trains for microstructural characterization. Transverse cross-sections from near the fuel foil midplane, see Figure 1 for an example, were prepared for optical microscopy (OM), which was conducted at $50\text{-}500\times$ objective magnifications. Additional adjacent cross-sections were prepared from select plates for scanning electron microscopy (SEM) characterization at the Irradiated Materials Characterization Laboratory (IMCL).

2.2.1 Calculating fuel swelling

As has been discussed in depth previously, constraint in the axial length and transverse width in plate-type fuel geometries result in the change in plate thickness being directly correlated to the volumetric swelling of the fuel foil [1, 10, 13], using equation (1)

where $t_{\text{post-plate}}$ is the post-irradiation plate thickness, $t_{\text{pre-plate}}$ is the pre-irradiation plate thickness, $t_{\text{pre-foil}}$ is the pre-irradiation fuel-foil thickness after roll-bonding the Zr diffusion barriers, t_{ox} is the post-irradiation oxide thickness, and t_{Zr} is the as-fabricated Zr diffusion barrier thickness per foil side. The constraint that allows for this direct relation between volumetric change and plate thickness is known to result in some fuel relocation at the fuel zone edges [10, 14], and thus artificially high swelling calculations using the above relation. However, it has been demonstrated that statistical methods may be employed in the analysis to mitigate this, discussed in the following section [10, 13].

During fabrication, the thickness was measured on a coordinate grid across the Zr roll-bonded U-Mo fuel foil and across the final fuel plates. As was detailed in a similar mini-plate study [13], the coordinate grids for each of these pre-irradiation thickness measurements were placed into the same reference frame as the BONA4INL measurement bench, and pre-irradiation plate and foil thickness values were interpolated via Delaunay triangulation for each PIE profilometry measurement. For PIE profilometry measurement locations outside the pre-irradiation measurement grid, values were extrapolated from the outer measurements in a “hull,” with extrapolation bounded by the maximum allowable fuel zone in the fabrication specification. While there is local variation in the Zr diffusion barrier thickness as a result of the fabrication process [3, 5], it is on the order of the BONA4INL measurement bench resolution, so the average Zr thickness for each foil was assumed to be constant over its respective roll-bonded foil, consistent with historical methods [10]. As in previous U-Mo plate fuel experiments irradiated in the ATR [10, 13], oxide growth was limited, as measured via eddy current and validated via OM and SEM, and on the order of the thickness resolution limit of the BONA4INL measurement bench. Therefore, the oxide correction term was neglected, allowing for the simplified equation (2) to be used to calculate the fuel swelling [13].

A fuel swelling fraction value should only be calculated from within the fuel zone; however, the fuel zones are known to not be 100% nominal. Therefore, a consistent swelling calculation data filter was implemented in addition to the geometric filter of the maximum specified fuel zone listed above, such that the fuel swelling fraction was only calculated in instances where plate thickness increased. As the minimum fission density in the MP-1 test train exceeds doses where irradiation-induced contraction may be observed, this filter effectively restricts fuel swelling calculations to fueled regions of the plates. It should also be noted that while the two B-plates with bond-line separations were included in this analysis, the thickness measurements from the areas surrounding the bond-line separation were excluded from the swelling calculations.

2.2.2 Coupling neutronics and PIE

To compare local fuel swelling fraction behavior to local calculated irradiation conditions, the end-of-life (EOL) fission density nodes from as-run neutronics calculations were placed into the PIE measurement reference frame at the nominal fuel zone location, consistent with the as-run simulations [6, 7, 8, 9]. The local EOL fission densities were then associated with each PIE measurement coordinate, using the same methods detailed in a prior mini-plate swelling analysis [13]. It should be noted that during the first cycle of medium power irradiations, it is known that the mini-plate test train was able to axially rotate in the south flux trap, and the neutronics modeling could only partially simulate this orientation shift. Since the general trend of low fission density swelling in monolithic U-10Mo is well understood [10], the orientation of the as-run nodes was placed consistent with the PIE observed thickness changes for these plates.

The individual MP-1 local swelling fraction and local fission density data pairs were consolidated into datasets by fabricator and fuel-foil geometry. The data pairs in the consolidated variable datasets were then shuffled and resorted by local fission density to remove any individual fuel plate or fuel foil geometric or constraint biases before being binned by every nearest 100 data points, as defined by local fission density. Quadratic fits, constrained through the origin, were then performed on both these binned datasets as well as their unbinned, raw data counterparts to allow for statistical comparisons using the 95% confidence bands and prediction bands from the fits. Extensive analysis of these empirical fitting and binning methods were conducted previously in the development of the currently recommended U-10Mo swelling model [10]. These methods have been employed previously in statistical comparison of swelling behavior between mini-plate fabrications [13], and as the methods reproduce those employed in the current U-10Mo swelling model development, direct comparison between the model and these results is possible.

In order to associate the DE-PIE microstructural observations with the fission density, the sectioning for each OM and SEM cross-section was placed into the same PIE measurement reference frame, with an assumed saw loss of 0.5 mm for each cut. The cross-section geometries were then coupled with the partially and fully overlapped as-run neutronics nodes in the same reference frame to determine the calculated minimum, maximum, and average EOL fission densities for each OM and SEM sample. A schematic illustrating this is included in Figure 1.

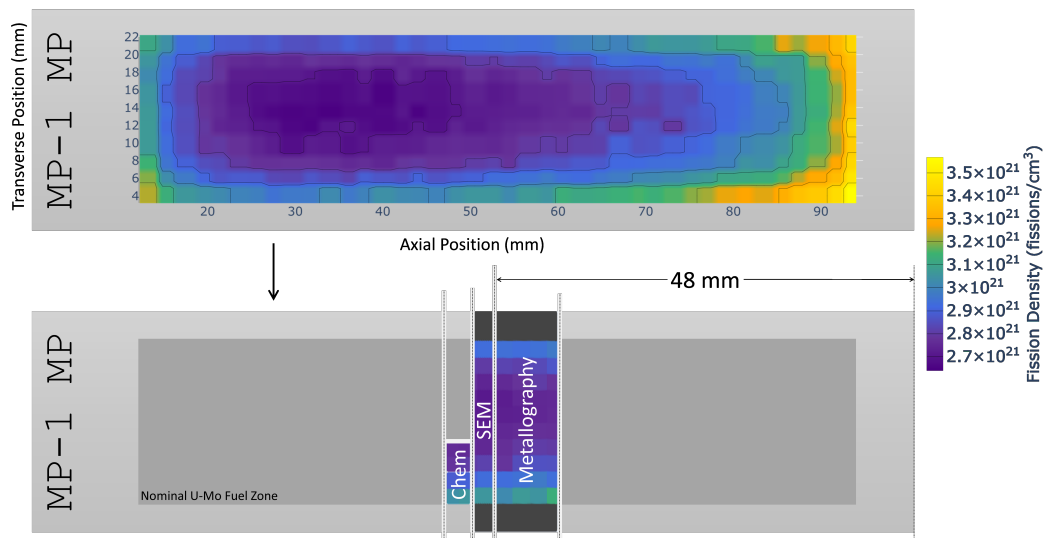


Figure 1 – Schematic illustrating coupling of mini-plate sectioning with end-of-life fission density nodes, calculated in the as-run neutronics analysis.

3. Results

3.1 Non-destructive Examination: Profilometry and Swelling

The raw local MP-1 swelling vs. fission density data are plotted in Figure 2(a) against the U-10Mo swelling model currently recommended by the USHPRR-FQ pillar, with its 95% confidence band and the upper and lower 95% prediction bounds for raw data, see Robinson et al. for model equations [10]. It is readily observable that the majority of data points for both the C and B-plates fall within the 95% prediction band, with constrained plate regions being the only outliers. Further, the swelling behavior for the non-delaminated regions of the two bond-line separated B-plates appears to be consistent with the swelling of other B-plates. Initial observations of the scatter suggest that the B-plate data may be consistently higher in swelling at a given fission density, relative to the C-plates.

Quadratic fits of the C and B consolidated datasets are plotted in Figure 2(b) with their 95% confidence and prediction bands, again with the U-10Mo swelling model and its confidence band. The binned consolidated datasets are also included to demonstrate the behavior with reduced visual scatter. It may be clearly observed that there is no overlap between the confidence bands of the C and B-plate fits for any of the fission densities tested. At low fission density the confidence band for the U-10Mo swelling model overlaps with the C-plate data, but diverges visibly at moderate fission densities, while retaining a consistent trend. This will be discussed further below.

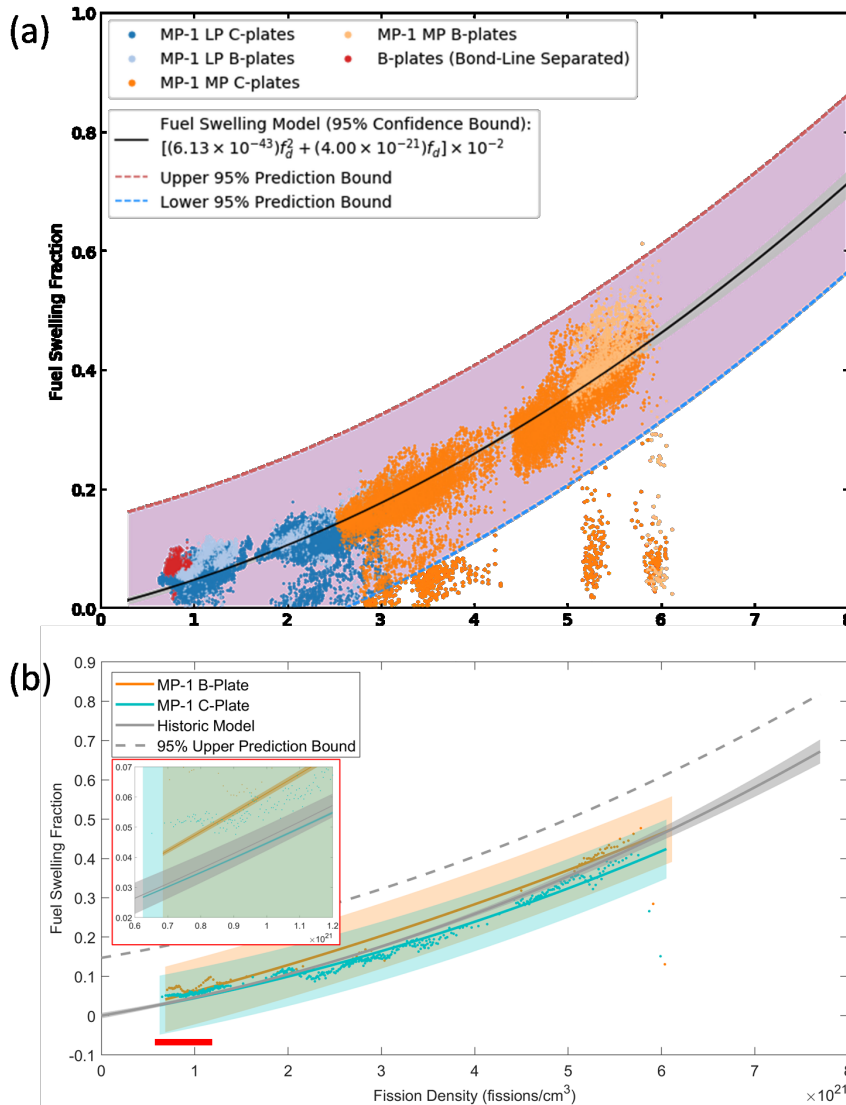


Figure 2 – Raw (a) and binned (b) MP-1 swelling and fission density data pairs, plotted against the currently recommended U-10Mo fuel swelling model [10] and its 95% confidence and prediction bands. Included in (b) are quadratic fits of the full C and B-plate consolidated datasets

3.2 Destructive Examination

3.2.1 Optical Microscopy

Optical metallography images of transverse cross-sections from MP-1 B and C-plates irradiated to multiple fission densities are shown in Figure 3 and Figure 4, respectively. In each case, the minimum and maximum fission densities for the transverse cross-sections imaged are reported with the microstructures as a range. It should be noted that the discoloration observed in the lowest fission density C-plate near the upper interface between the fuel foil and Zr diffusion barrier is an artifact of sample preparation and should be disregarded. A different microstructural evolution may be readily observed between the two figures. Examining the C-plates in Figure 3, minor micron-scale fission gas bubbles are

resolvable at the grain boundaries at lower fission densities ($2-3 \times 10^{21}$ fissions/cm³). Above 3×10^{21} fissions/cm³ grain refinement is observed with grain subdivision occurring, growing the high burn-up, fission gas porous structure in the grain boundaries. The highest fission density C-plate exhibits a majority of this high burn-up structure (HBS) [2, 15] with islands of remaining grains. By contrast, the similar fission density B-plate in Figure 4 shows a fully recrystallized HBS with extensive fission gas porosity. At lower fission densities, a non-uniformity in polished surface oxidation of the B-plate fuel foil is observed, which appears to be present in the fully recrystallized structure as well; though, the contrast is more difficult to observe in the porous HBS. At the lower fission densities this contrast heterogeneity appears to coincide with clusters of micron-scale fission gas porosity, but the higher magnification SEM analysis in the following section is needed to resolve this.

C - Plates

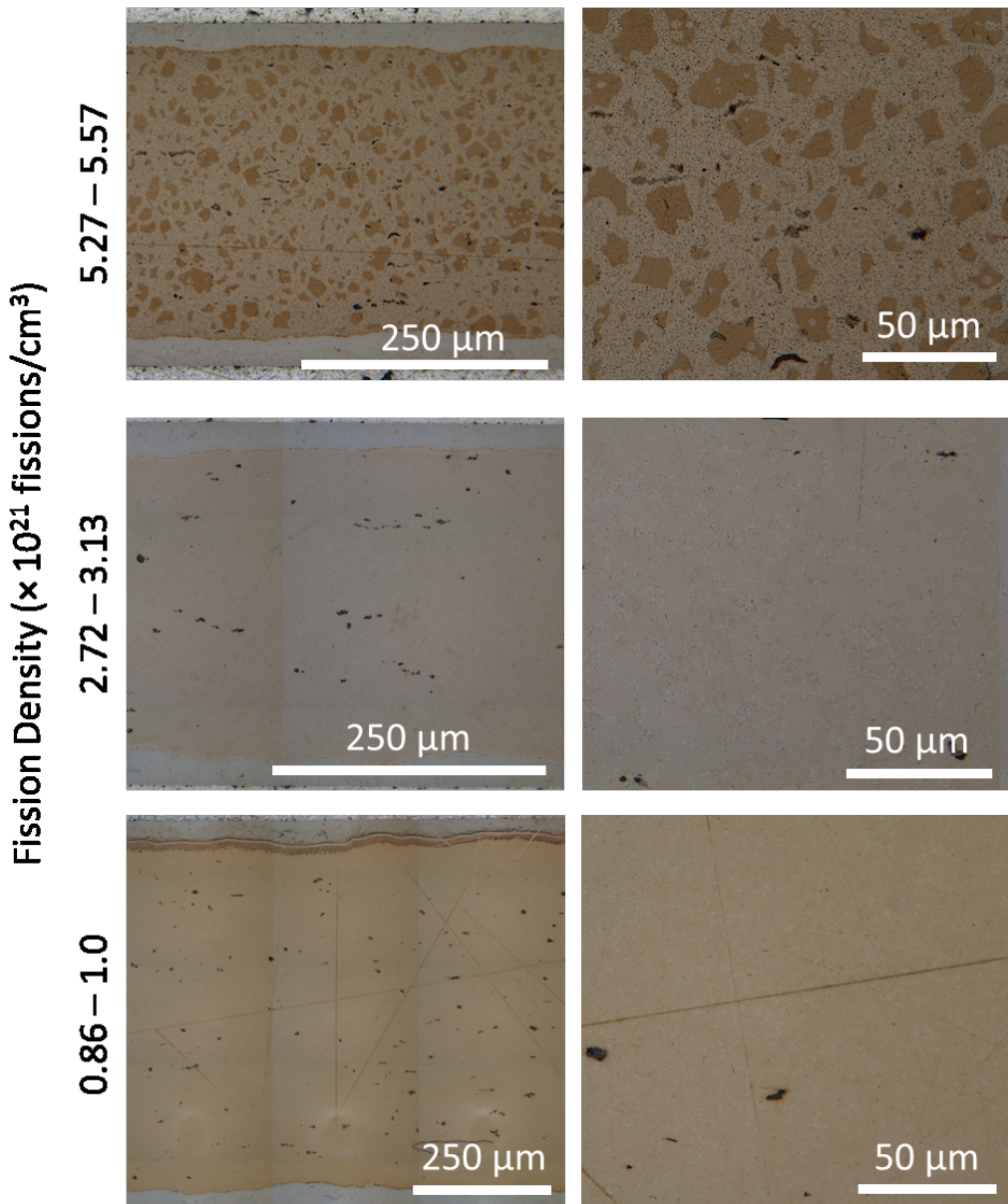


Figure 3 – Low and high magnification optical metallography from MP-1 C-plates irradiated to increasing fission densities, detailed as the upper and lower bounds for the transverse cross-section

It should be acknowledged that secondary phases ($\sim 10\ \mu\text{m}$) similar to carbides are observed at all fission densities. In this work, these are most easily observed in the high magnification, high fission density C-plate in Figure 3. These secondary phase impurities have been observed previously in both as-fabricated and irradiated conditions [2, 5, 16, 17]. While fission gas porosity has been observed at their interfaces with the fuel, the bubble morphology does not appear significantly different from the porosity of the HBS [17]. A separate study investigating the impact of carbide impurity interface evolution is ongoing.

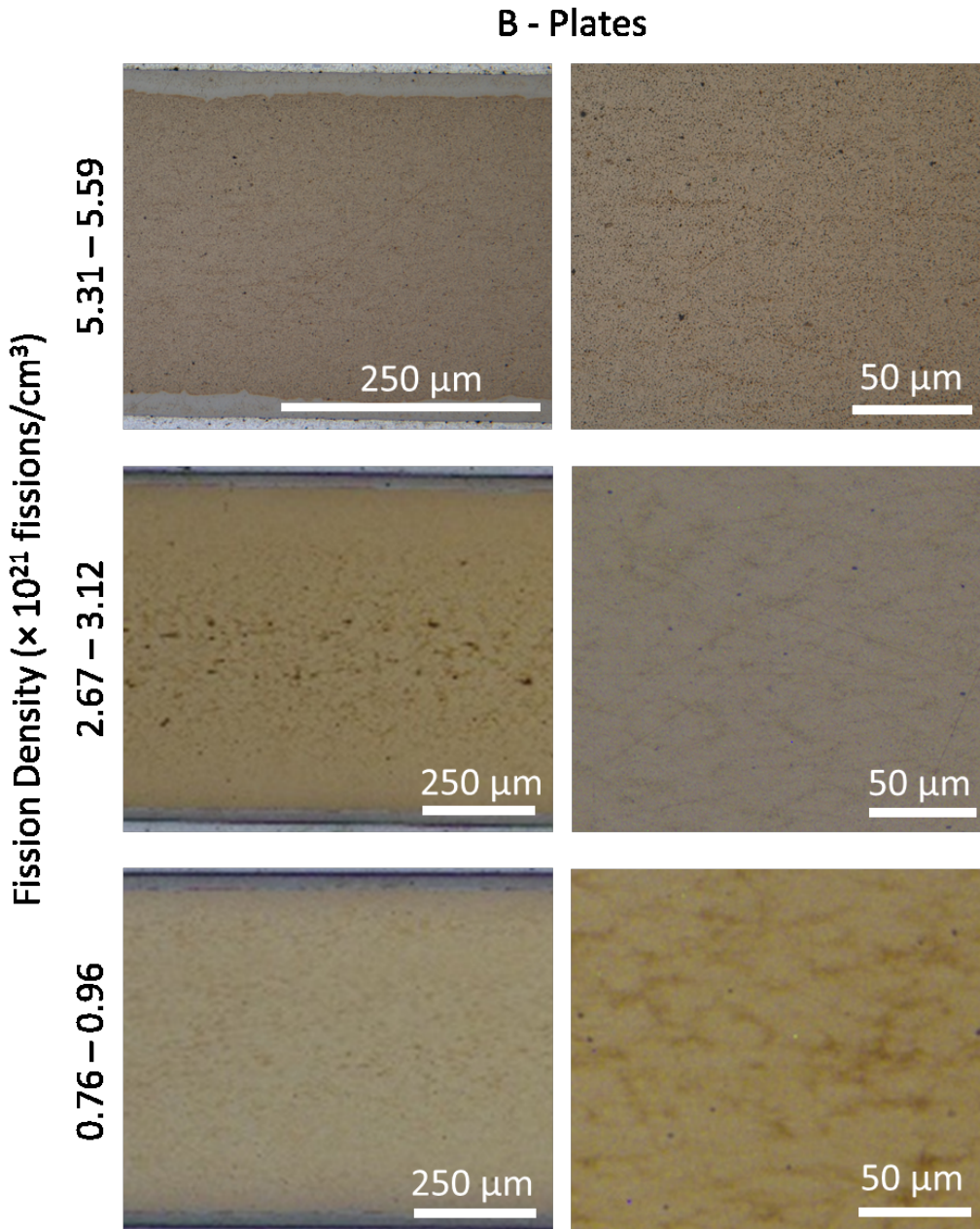


Figure 4 – Low and high magnification optical metallography from MP-1 B-plates irradiated to increasing fission densities, detailed as the upper and lower bounds for the transverse cross-section

3.2.2 SEM

Back-scatter electron (BSE) imaging of cross-sections as well as high resolution BSE imaging of large-area lift-outs (LALOs) for MP-1 C and B-plates of increasing fission densities are shown in Figure 5 and Figure 6, respectively. Examining Figure 5, it is possible to readily resolve the micron-scale fission gas porosity accumulating at the boundaries of equiaxed grains at low fission density. As in the OM imaging in the previous section, with increasing fission density this accumulation continues and at moderate fission densities ($>3 \times 10^{21}$ fissions/cm³) grain refinement is observed. At the highest fission density, the majority of the grains are refined to the fission gas porous HBS, with some islands of the original grains remaining.

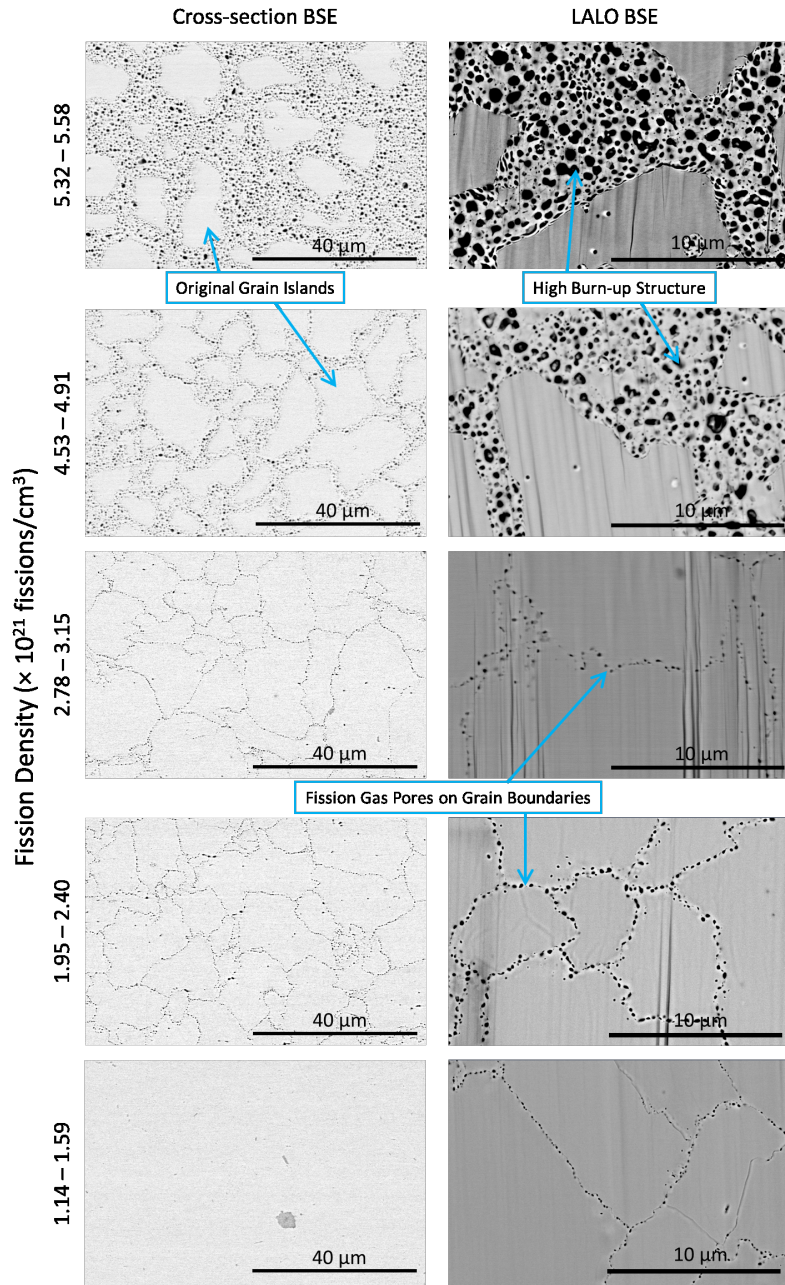


Figure 5 – Backscatter SEM imaging of cross-sections and LALOs from MP-1 C-plates irradiated to increasing fission densities, detailed as the upper and lower bounds for the cross-section

In Figure 6, the BSE Z-contrast readily reveals regions of varied average Z, with brighter BSE intensity regions previously identified in this material as having low-Mo [17, 18]. In the low fission density sample, these regions appear to have smaller grain clusters present with fission gas porosity precipitated on the higher density of grain boundaries. The highest fission density sample again shows the low-Mo chemical banding; although, the grain structure is fully refined to the HBS of larger fission gas porosity [15]. It should be noted that in both highest fission density the C and B-plates in Figure 5 and Figure 6, respectively, very limited bubble interconnection is observed.

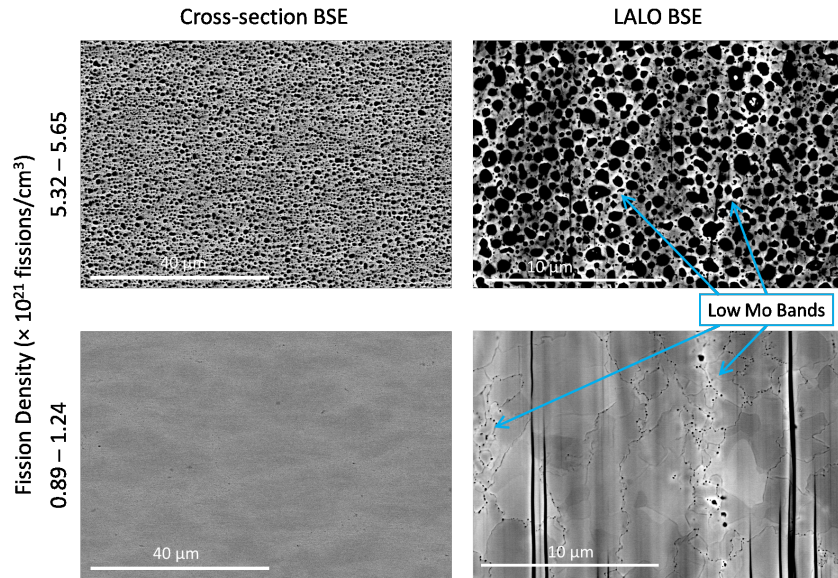


Figure 6 – Backscatter SEM imaging of cross-sections and LALOs from MP-1 B-plates irradiated to increasing fission densities, detailed as the upper and lower bounds for the cross-section

4. Discussion

4.1 Differences in swelling response

Examining Figure 2(a), the MP-1 fuel swelling appears consistent with the predictions of the monolithic U-10Mo swelling model currently recommended by the USHPRR-FQ pillar [1, 10]. It should be noted that the comparisons that may be made using prediction and confidence bands are distinct. Prediction bands are an indication of probability of where the next datapoint may appear [19]. With this in mind, the consistency of the ~47,000 MP-1 data points within the 95% prediction band of the currently recommended U-10Mo swelling model is consequential for both this experiment and the model. There are two observations that can be drawn from these results; first, the MP-1 swelling behavior appears to be consistent with the historical U-10Mo irradiation experiments, despite being the first mini-plates fabricated commercially at scale. Second, the model proposed by Robinson et al., developed using ~18,000 swelling data pairs, was able to conservatively predict the behavior of the significantly larger MP-1 dataset.

On the other hand, confidence bands indicate the degree of confidence in the empirical fit of the data, and wherever the confidence bands of two models overlap, a statistical difference between those models cannot be distinguished [19]. This is the case for the C-plate model and the currently recommended U-10Mo model in the low fission density range Figure 2(b) inset. By contrast, a lack of overlap between

two model 95% confidence bands, such as between the B-plates and both the historical and C-plate models in the Figure 2(b) inset, indicates a detectable and statistically relevant difference between the models [19]. Therefore, the non-overlapping confidence bands between the B and C-plates at all tested fission densities confirms the initial observation in Figure 2(a); there is increased swelling observed in the B-plates relative to the C-plates at these regimes. It should be acknowledged that while this difference is statically quantifiable, it is admittedly small. Though the models are parallel, and neither overlaps within the fission density regimes tested, each binned data point falls within the 95% prediction band of the other consolidated dataset model. This suggests consistent and stable swelling behavior in both fuel plate fabrications, despite some mechanism offsetting the trends.

It is noteworthy that there is divergence between the C-plate model and the currently recommended U-10Mo model at moderate fission densities, with a detectibly lower swelling behavior observed in the MP-1 C-plates at higher fission densities. Further, the recommended U-10Mo model overlaps the B-plate model at the highest fission density tested in the MP-1 experiment. Several factors could explain the source of this behavior; however, an exploration of the mechanisms behind the systematic B and C-plate offset will aid in this discussion.

4.2 Microstructural evolution in B and C-plates

The general microstructural evolution in the MP-1 experiment appears consistent with the well-established U-Mo fuel system behavior [1, 10, 20]. Examining the C-plates in Figure 3 and Figure 5, at low fission densities ($<3 \times 10^{21}$ fissions/cm³), fission gas bubbles are only observed in OM and SEM to precipitate at grain boundaries, which is expected. At low fission density, the original grain boundaries serve as sinks and precipitation sites for micron-scale fission gas bubbles while the fission gas inventory interior to the grains is retained in a FCC gas super lattice [20, 21, 22, 23]. At intermediate fission density, the grains begin to refine, starting from their original grain boundaries and forming an HBS [15]. In U-Mo, this is linked to the collapse of the fission gas super lattice and coalescence of additional micron-scale fission gas porosity in the newly formed sub-grain boundaries [10, 23]. At the highest fission density experienced in the MP-1 C-plates in Figure 3 and Figure 5, this high burn-up phase is observed as the primary phase with only small islands of the largest initial grains remaining.

By contrast in Figure 4 and Figure 6, only a fully refined HBS is observed in the B-plates at a similar fission density ($\sim 5.43 \times 10^{21}$ fissions/cm³). The fission gas porosity in this phase also appears to be formed into larger bubbles than in the C-plates, similar to the highest burn-up progression reported previously [10]. A separate localized study confirmed that, on average, larger diameter pores were observed in the HBS phase in the B-plates but also noted the total area fraction difference in the porosity is subtle [17]. It appears that the microstructural refinement in the B-plates is at a later stage than in C-plates at this higher fission density regime, with less of the fission gas inventory retained in the super lattice in unrefined grain interiors. This seems a plausible explanation for the difference in swelling behavior at similar fission densities observed in this study. However, it is important to emphasize that despite this, neither the B nor C-plates demonstrate significant fission gas porosity interconnection that might suggest an imminent unstable breakaway swelling regime [10]. Rather the bubbles, though apparently larger in the B-phase, appear discrete and stable, consistent with the stable swelling regime observed in both models in Figure 2b.

Unfortunately, there were no B-plates in the MP-1 experiment within the moderate refinement fission density regime, so changes observed at lower fission densities must be interpolated to the known refined HBS. In both lower fission density plates examined in Figure 4, there is extensive heterogenous oxidation of the fuel foil, suggesting some phase variation that appears to have some fission gas porosity

present; though, the resolution limits direct observation. That said, BSE SEM at the lowest fission density regimes reveal BSE intensity banding in these phases, consistent with Mo inhomogeneity chemical banding observed previously in both unirradiated and irradiated material [5, 17, 18]. In the unirradiated fuel, these regions of low Mo were observed to decompose from the γ -U-Mo phase to less stable α -U-Mo phase [5], which is consistent with U-Mo that was not fully homogenized during the alloying process [24]. At low and high fission densities, the chemical banding remains, and for the low burn-up B-plate, regions of brighter BSE intensity (lower Mo content) exhibit micron-scale grains. Previous analysis of highly localized regions of this plate suggested irradiation assisted refinement of the α -U-Mo phase to the γ -U-Mo phase as a mechanism for this reduced grain formation [18]. It should be emphasized that these micron-scale grains were not present in the initial microstructure, and the homogenized C-plates did not have a substantially larger initial average grain size [5]. However, the increased initial α -U-Mo phase decomposition regions combined with the irradiation assisted γ -U-Mo phase reformation appears to result in bands of micron-scale grains in the B-plates at lower fission densities than those needed for the grain refinement process discussed previously [10, 23]. These micron-scale grain regions naturally result in an increased grain boundary density, each of which may be decorated with micron-scale fission gas bubbles. This confirms the potential fission gas porosity observed in the lower resolution OM imaging at low-to-moderate fission densities. It should be reiterated that no chemical banding is observed in the C-plates over the fission density regime examined in MP-1, consistent with an initially homogenized microstructure [5] and localized irradiated analyses [17, 18].

4.3 Influence of microstructural homogeneity on swelling

It seems likely that the homogenization anneal employed during the fabrication of the C-plates resulted in the observed uniform Mo distribution and the expected U-10Mo microstructural evolution with fission density. Further, it appears that B-plates lacking this homogenization anneal step led to the increased micron-scale fission gas porosity at lower fission densities ($<3 \times 10^{21}$ fissions/cm³), through an increase in grain boundaries to serve as sinks for disordered fission gas inventory coalescence. The additional fission gas porosity seems a plausible explanation for the increased swelling observed at lower fission densities in Figure 2b, preceding any grain refinement that typically allows for this porosity formation. This essentially offsets the fission gas swelling regime to lower fission densities [10], and a highlight of this comparison is shown in Figure 7. Additionally, a seeded micron-grain microstructure would likely lead to a fully refined HBS in advance of homogenized C-plates, as is readily observed in the high burn-up comparison in Figure 7. Therefore, the homogenization anneal appears to result in a measurable, albeit small, reduction in fuel swelling in the MP-1 experiment at all fission densities tested.

Now that a plausible explanation is proposed for the observed offset behavior in the MP-1 B and C-plates, the differences between their models and those of the currently recommended U-10Mo swelling model may be explored. Again, it should be emphasized that the prediction band of the current model does predict both the B and C-plate behavior. However, the current model's confidence band diverges from overlapping the C-plate behavior at moderate fission densities before overlapping the B-plate model at the highest fission density examined in the MP-1 experiment. One possible explanation for this deviation may simply be due to data density at fission density regimes exceeding 5×10^{21} fissions/cm³. The currently recommended swelling model was developed with over 18,000 data pairs; however, an order of magnitude more data pairs are available in the MP-1 dataset at this higher fission density regime (~8,500 vs. 850 data pairs) [10]. It is possible that the higher MP-1 C-plate data density at this regime may be revealing a more accurate, reduced swelling behavior for this regime; however, given the proposed explanation for the systematic variation between C and B-plates, another explanation seems more plausible.

The currently recommended swelling model was developed as an empirical quadratic fit of binned fuel swelling and fission density data pairs. Extensive analysis was conducted to down-select this statistical fitting method, documented in Robinson et al. [10]. Included in the model dataset are ~18,000 data pairs from different fabricated experiments, which show sufficient agreement to warrant their inclusion in the model. However, the results above indicate that with sufficient data density, it is possible to detect subtle changes in behavior due to a fabrication variable, such as the homogenization anneal, a relatively late addition to the U-10Mo fabrication process [3]. Only two of the historical experiments included in the model dataset received a separate homogenization anneal, the AFIP-6MKII and AFIP-7 full size plate experiments. Each experiment encompassed different fission density regimes, with AFIP-7 at low to moderate conditions ($\sim 1.5 - 3 \times 10^{21}$ fissions/cm³), and AFIP-6MKII reaching a higher burn-up at a higher power density ($\sim 4 - 5.5 \times 10^{21}$ fissions/cm³). Examining the AFIP-7 as-fabricated and irradiated microstructure, it appears homogeneous with a similar fission gas porosity as observed at comparable burn-up MP-1 C-plates [1, 10]. Additionally, though the AFIP-3BZ plate ($\sim 2.5 - 4.5 \times 10^{21}$ fissions/cm³) did not receive an explicit homogenization anneal, its microstructure appears homogenous, and its evolution appears consistent with comparable burn-up MP-1 C-plates [1]. When the swelling behavior observed in AFIP-7 and AFIP-3BZ plates [10] are compared with those presented here, they appear in-line with the MP-1 C-plates. In-fact, the fission density regime where the confidence band of the U-10Mo swelling model overlaps and closely parallels the MP-1 C-plates corresponds to where the model is contributed to by the >6,700 data-pairs from AFIP-7 and AFIP-3BZ in those regimes.

Conversely, despite the AFIP-6MKII experiment receiving a homogenization anneal, unirradiated fuel analysis of archive material revealed a heterogeneous microstructure [25, 26, 27], similar to that observed in the MP-1 B-plates [5, 17, 18, 28]. Irradiated fuel cross-sections from conditions intermediate to those examined in the B-plates in this work also appear to illustrate a microstructural evolution between the stages available from B-plates, see example in Figure 7. It should be noted that the AFIP-6MKII experiment is the primary contributor to the current U-10Mo swelling model for this regime (1950 swelling vs. fission density data pairs). Given this weighting and the microstructural behavior, this seems a plausible explanation for the divergence of the current U-10Mo swelling model from C-plate behavior to converge with the confidence band of the B-plate model in this regime. Further, if a quadratic model of the historical swelling data that excludes the AFIP-6MKII is examined in Figure 7, its confidence band has better agreement with those of the C-plate model for the fission densities examined. It should be acknowledged that there are likely other contributing factors beyond the heterogeneous microstructure that may explain the AFIP-6MKII weighting of the model toward the heterogeneous MP-1 B-plate behavior, such as power density, fuel centerline temperature variation, and pre-irradiation impurity precipitates. However, the microstructure heterogeneity may partially explain the lack of full agreement between the AFIP-6MKII swelling profilometry and its local fission density peaking [28, 29] and would also explain why a weighting from this experiment would lead to an intersection that crosses the B-plate model rather than a parallel overlap of trends.

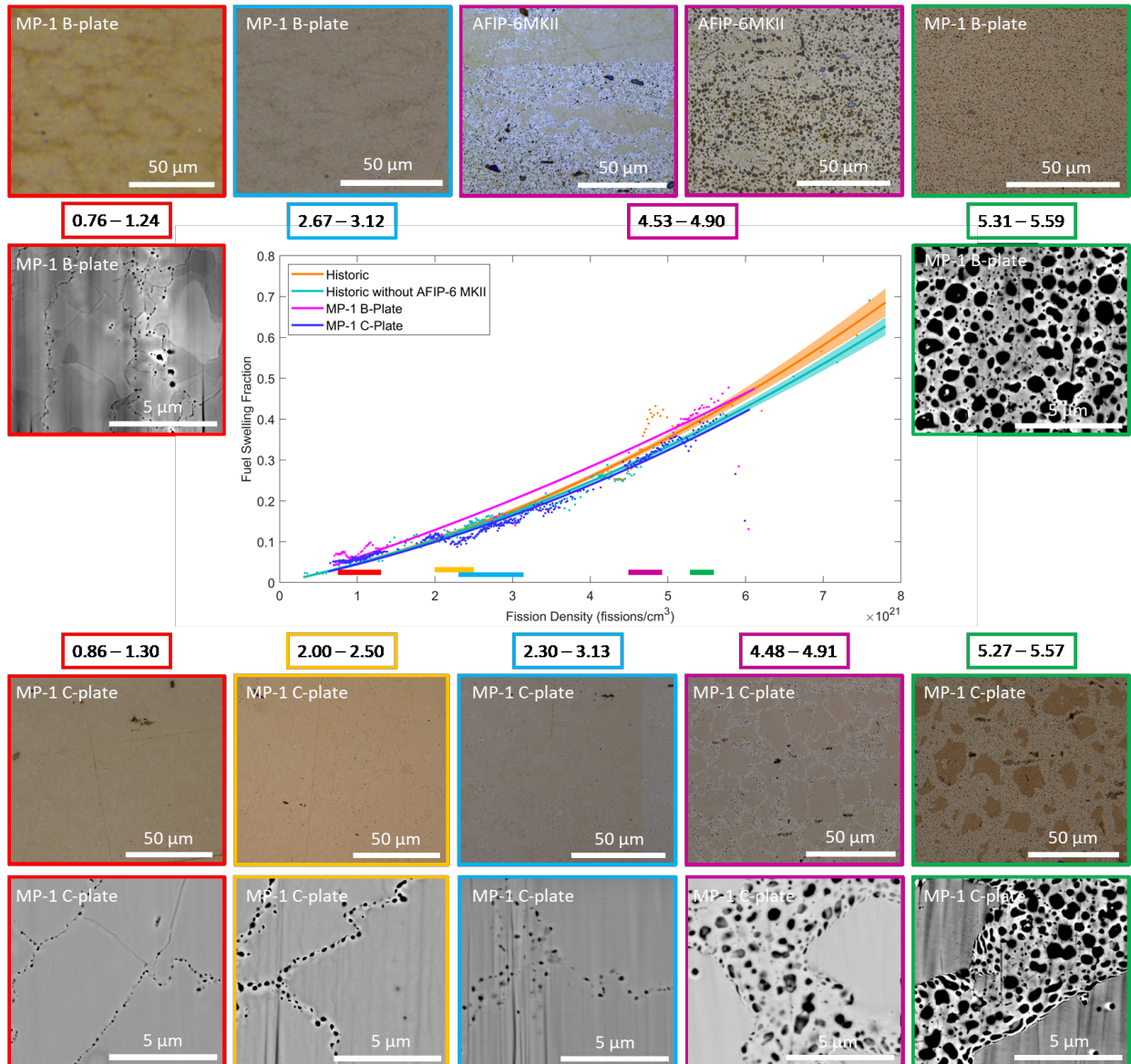


Figure 7 – Quadratic fits of MP-1 C and B-plate swelling vs. fission density data pairs plotted against the currently recommended U-10Mo empirical swelling models based on the historical data including and excluding the AFIP-6MKII experiment. Also included are OM and SEM images from the MP-1 C and B-plates as well as AFIP-6MKII for reference with colored bars indicating the approximate fission density regime encompassed by the cross-sections.

It is the recommendation of the authors that the full, currently recommended U-10Mo swelling model [10], based on the historic datasets, be maintained as a conservative estimate of swelling until a final swelling model may be developed from the forthcoming U-10Mo qualification experiments. While the MP-1 C-plate fabrication is closely representative of the down-selected fuel heat treatment design, the current historical model fully predicted both the B-plate and C-plate data scatter. This suggests the upper prediction bound is sufficiently conservative, such that fuel swelling response to varied initial fabrication conditions are equally predicted. A final U-10Mo swelling model will be developed from the substantial data anticipated from the qualification experiments, and at that time the MP-1 and historic datasets will be

evaluated for their appropriate statistical inclusion or exclusion.

5. Conclusions

Fuel swelling and microstructural evolution were compared within the MP-1 experiment. Good overall agreement was observed between the MP-1 swelling behavior and those of historical U-10Mo experiments. The currently recommended swelling model predicted the upper bounds of scatter in both MP-1 B and C-plates, despite a statistical offset in these two fabrications being detected. Optical metallography and SEM suggest that the high swelling offset of the B-plate behavior is due primarily to regions of micron-scale recrystallized grains providing increased sites for early precipitation of micron-scale fission gas porosity. Conversely, the initially homogeneous C-plate microstructure evolves as expected with grains refining and the HBS forming in an increasing phase fraction at the grain boundaries with increasing fission density. Comparing with the microstructures that most heavily contribute to the currently recommended U-10Mo swelling model validates this behavior. The homogenous initial microstructure in the AFIP-7 dominated regime is consistent with where the model overlaps the C-plate behavior, whereas the AFIP-6MKII regime diverges, likely due partially to its initial heterogeneous microstructure. It is important to emphasize that in both the MP-1 B and C-plates there was not evidence found of an imminent breakaway swelling regime. The offsets in behavior measured in this study are subtle, and it is only through the density of data in the MP-1 experiment that it was possible to detect that the swelling behavior appears to be statistically offset by a homogeneous initial microstructure. That said, the effect is mechanistically consistent and when compared with historical behavior demonstrates that the swelling phenomena within the U-10Mo system is stable and predictable. A final model will be developed from the forthcoming U-10Mo qualification experiments, and until that time the swelling model developed by Robinson et al. that includes all the historic datasets is still recommended as a conservative estimate of the swelling behavior. Additionally, future work to utilize image analysis to better understand the fission gas porosity evolution is anticipated.

U.S. Department of Energy Disclaimer

This information was prepared as an account of work sponsored by an agency of the U.S. Government. Neither the U.S. Government nor any agency thereof, nor any of their employees, makes any warranty, express or implied, or assumes any legal liability or responsibility for the accuracy, completeness, or usefulness of any information, apparatus, product, or process disclosed, or represents that its use would not infringe privately owned rights. References herein to any specific commercial product, process, or service by trade name, trademark, manufacturer, or otherwise, does not necessarily constitute or imply its endorsement, recommendation, or favoring by the U.S. Government or any agency thereof. The views and opinions of authors expressed herein do not necessarily state or reflect those of the U.S. Government or any agency thereof.

Declaration of Competing Interests

The authors declare that they have no known competing interests, whether financial, personal, or relational, that could have or appeared to influence the work reported in this paper.

CRedit authorship contribution statement

W.A. Hanson: Conceptualization, Methodology, Investigation, Data Curation, Formal analysis, Visualization, Writing – Original and Revised drafts. **D. Salvato:** Investigation, Data Curation, Formal

analysis, Visualization, Writing – Review & Editing. **A.B. Robinson:** Conceptualization, Methodology, Investigation, Data Curation, Formal analysis, Supervision, Writing – Review & Editing. **N.J. Lybeck:** Methodology, Data Curation, Formal analysis, Visualization, Writing – Review & Editing. **J.-F. Jue:** Conceptualization, Data Curation, Formal analysis, Visualization, Writing – Review & Editing. **T.L. Trowbridge:** Investigation, Writing – Review & Editing. **J. Burns:** Investigation, Writing – Review & Editing. **F.G. Di Lemma:** Investigation, Writing – Review & Editing. **C.A. Smith:** Investigation, Visualization, Writing – Review & Editing. **M.A. Marshall:** Conceptualization, Visualization, Writing – Review & Editing. **D.D. Keiser Jr.:** Conceptualization, Formal analysis, Supervision, Writing – Review & Editing. **J.J. Giglio:** Conceptualization, Project administration, Funding acquisition, Supervision, Writing – Review & Editing. **J.I. Cole:** Conceptualization, Project administration, Funding acquisition, Supervision, Writing – Review & Editing.

Acknowledgements

This work is supported by the U.S. Department of Energy, under DOE Idaho Operations Office Contract DE-AC07-05ID14517. Accordingly, the U.S. Government retains a nonexclusive, royalty-free license to publish or reproduce the published form of this contribution, or allow others to do so, for U.S. Government purposes.

This work is dedicated to the memory of Dr. Dennis D. Keiser Jr., whose mentorship in characterization of U-Mo fuels was integral to the discussion in this work. The authors would also like to acknowledge the staff, engineers, and operators of the INL Materials and Fuels Complex (MFC) Hot Fuel Examination Facility (HFEF), Irradiated Materials Characterization Laboratory (IMCL), and Electron Microscopy Laboratory (EML) for their efforts during the post-irradiation examinations; specifically, G. C. Papaioannou and B. K. Allen for their work on the BONA4INL measurement bench and John Stanek, Addi Quintillano, Brian Frickey, Shane Haney, Samuel Powderly, and Scott Anderson for their assistance in the cross-section preparations.

6. References

- [1] B. Rabin, M. Meyer, J. Cole, I. Glagolenko, W. Jones, J.-F. Jue, D. Keiser Jr, C. Miller, G. Moore, H. Ozaltun, F. Rice, A. Robinson, J. Smith, D. Wachs, W. Williams, N. Woolstenhulme, G. Hofman and Y. Kim, "Preliminary Report on U-Mo Monolithic Fuel for Research Reactors," *INL/EXT-17-40975, Revision 4, Idaho National Laboratory*, April 2020.
- [2] T. Ajantiwalay, C. Smith, D. D. Keiser and A. Aitkaliyeva, "A critical review of the microstructure of UeMo fuels," *Journal of Nuclear Materials*, vol. 540, no. 152386, 2020, doi:10.1016/j.jnucmat.2020.152386.
- [3] L. Hubbard, C. Arendt, D. Dye, C. Clayton, M. Lerchen, N. Lombardo, C. Lavender and A. Zacher, "U-10Mo Baseline Fuel Fabrication Process Description," *Pacific Northwest National Laboratory, PNNL-26880*, Sep 2017, doi: 10.13140/RG.2.2.28508.54400.
- [4] S. M. Kilby, M. A. Marshall, D. O. Choe, J. W. Barney, G. L. Hawkes, C. Jensen, M. Lilo, I. Y. Glagolenko and J. I. Cole, "Design of Mini-Plate-1 Irradiation Test for Qualification of High-Density, Low-Enriched U-10Mo Monolithic Fuel," *JOM*, 2024, doi:10.1007/s11837-024-06954-z.
- [5] F. Di Lemma, J. Jue, A. Winston, X. Pu, S. Anderson, D. Keiser, J. Giglio and J. Cole, "Impacts of annealing treatment on the microstructure of U-Mo monolithic fuel plates," *Journal of Nuclear Materials*, vol. 564, no. 153687, 2022, doi:10.1016/j.jnucmat.2022.153687.
- [6] D. O. Choe, P. E. Gilbreath, P. F. O'Donnell, N. D. Meacham, J. L. Peterson-Droogh and M. A. Marshall, "As-Run Analysis for th MP-1 Low Power Experiment in the ATR Large B Position (B-10) through Cycle 164A and 164B," *ECAR- 5656, Rev. 0, Idaho National Laboratory*, 2021.

- [7] D. O. Choe, P. E. Gilbreath, P. F. O'Donnell, N. D. Meacham, J. L. Peterson-Droogh and M. A. Marshall, "MP-1 As-Run Low Power Physics Analysis in the ATR Large B Position (B-11)," *ECAR-5657, Rev. 0, Idaho National Laboratory*, 2021.
- [8] D. O. Choe, P. E. Gilbreath, P. F. O'Donnell, N. D. Meacham, J. L. Peterson-Droogh and M. A. Marshall, "MP-1 As-Run Low Power Physics Analysis in the ATR Large B Position (B-12)," *ECAR-5069, Rev. 1, Idaho National Laboratory*, 2021.
- [9] D. O. Choe, P. E. Gilbreath, P. F. O'Donnell, N. D. Meacham, J. L. Peterson-Droogh and M. A. Marshall, "As-Run Analysis for the MP-1 Medium Power Experiments Ccles 164B and 166," *ECAR-5658, Rev. 0, Idaho National Laboratory*, 2021.
- [10] A. Robinson, W. Williams, W. Hanson, B. Rabin, N. Lybeck and M. Meyer, "Swelling of U-Mo Monolithic Fuel: Developing a Predictive Swelling Correlation under Research Reactor Conditions," *Journal of Nuclear Materials*, vol. 544, pp. 1-12, 2020, doi:10.1016/j.jnucmat.2020.152703.
- [11] M. A. Marshall, J. I. Cole, I. Glagolenko, W. A. Hanson, J.-F. Jue, A. B. Robinson and J. A. Smith, "MP-1 Experiment Recovery Report, Fuel Breach and Reinsertion Risk Assessment," *INL EXT-20-57170, Revision 0, Idaho National Laboratory*, June 2020.
- [12] J. Cole, N. Cordes, F. Di Lemma, D. Frazer, J. Giglio, M. Johnson, J. Locke, G. Moore, H. Ozaltun, T. Trowbridge and Y. Sohn, "USHPRR MP-1 Irradiation Test: Assessment of Edge Pitting and Bond Line Corrosion in Vendor Produced Fuel Plates," *INL/EXT-21-61324, Rev. 0, Idaho National Laboratory*, June 2021.
- [13] W. A. Hanson, A. B. Robinson, N. J. Lybeck, J. W. Nielsen, B. Ye, Z.-G. Mei, D. D. Keiser Jr., L. M. Jamison, G. L. Hofman, A. M. Yacout, A. Leenaers, B. Stepnik and I. Glagolenko, "Non-destructive analysis of swelling in the EMPIRE fuel test," *Journal of Nuclear Materials*, vol. 564, no. 153683, 2022, doi:10.1016/j.jnucmat.2022.153683.
- [14] A. Leenaers, S. Van den Berghe and C. Detavernier, "Surface engineering of low enriched uranium-molybdenum," *Journal of Nuclear Materials*, vol. 440, pp. 220-228, 2013, doi:10.1016/j.jnucmat.2013.04.068.
- [15] A. Leenaers, W. Van Rentergham and S. Van den Berghe, "High burn-up structure of U(Mo) dispersion fuel," *Journal of Nuclear Materials*, vol. 476, pp. 218-230, 2016, doi:10.1016/j.jnucmat.2016.04.035.
- [16] F. Di Lemma, J. Burns, J. Madden, A. Winston, A. Robinson, J. Jue, D. Deiser and J. Cole, "Texture analyses and microstructural evolution in monolithic U-Mo nuclear fuel," *Journal of Nuclear Materials*, vol. 544, no. 152677, 2021, doi:10.1016/j.jnucmat.2020.152677.
- [17] F. Di Lemma, T. Trowbridge, J. Jue, D. Salvator, A. S., C. Smith, B. Miller, D. Keiser, J. Giglio and J. Cole, "Effect of heat treatment on the microstructure of medium burn-up U-Mo monolithic fuel foils," *Journal of Nuclear Materials*, vol. 593, no. 155002, 2024, doi:10.1016/j.jnucmat.2024.155002.
- [18] F. Di Lemma, J. Jue, T. Trowbridge, C. Smith, B. Miller, D. Keiser, J. Giglio and J. Cole, "Annealing influence on the microstructure of irradiated U-Mo monolithic fuel foils," *Nuclear Materials and Energy*, vol. 35, no. 101436, 2023, doi:10.1016/j.nme.2023.101436.
- [19] W. Q. Meeker, G. J. Hahn and L. A. Escobar, *Statistical Intervals: A Guide for Practitioners and Researchers*, 2nd Edition, Hoboken, NJ: John Wiley & Sons, Inc., April 2017.
- [20] A. Leenaers, S. Van den Berghe, E. Koonen, V. Kuzminov and C. Detavernier, "Fuel swelling and interaction layer formation in the SELENIUM Si and ZrN coated U(Mo) dispersion fuel plates irradiated at high power in BR2," *Journal of Nuclear Materials*, vol. 458, pp. 380-393, 2015, doi:10.1016/j.jnucmat.2014.12.073.
- [21] C. Smith, K. Bawane, D. Salvato, M. Bachhav, D. Keiser, B. Miller, J. Gan, D. Choe, P. Gilbreath and W. Hanson, "Early self-organization of fission gas bubble superlattice formation in neutron-irradiated monolithic U-10Mo fuels," *Journal of Nuclear Materials*, vol. 578, no. 154358, 2023,

doi:10.1016/j.jnucmat.2023.154358.

- [22] J. Gan, J. D. D. Keiser, B. D. Miller, A. B. Robinson, D. M. Wachs and M. K. Meyer, "Thermal Stability of Fission Gas Bubble Superlattice in Irradiated U-10Mo Fuel," *Journal of Nuclear Materials*, vol. 464, pp. 1-5. doi:10.1016/j.jnucmat.2015.04.023, 2015.
- [23] J. Gan, B. D. Miller, D. D. Keiser Jr., J. F. Jue, J. W. Madden, A. B. Robinson, H. Ozaltun, G. Moore and M. K. Meyer, "Irradiated microstructure of U-10Mo monolithic fuel plate at very high fission density," *Journal of Nuclear Materials*, vol. 492, pp. 195-203. doi:10.1016/j.jnucmat.2017.05.035, 2017.
- [24] D. Burkes, R. Prabhakaran, T. Hartmann, J. Jue and F. Rice, "Properties of DU-10 wt% Mo alloys subjected to various post-rolling heat treatments," *Nuclear Engineering Design*, vol. 240, pp. 1332-1339, 2010, doi:10.1016/j.nucengdes.2010.02.008.
- [25] K. Verner, C. Smith, D. D. Keiser Jr., A. Aitkaleyva, B. Beeler and B. Miller, "AFIP6-MkII and RERTR-12 Porosity Data Collection and Analysis for Modeling and Simulation," *Idaho National Laboratory, INL/EXT-20-60135*, April 2020.
- [26] C. Smith, J. Jue, T. Trowbridge, D. Keiser, J. Madden, A. Robinson and J. Giglio, "Possible impacts of Mo chemical banding and second phase impurities on the irradiation behavior of monolithic U-10Mo fuels," *Journal of Nuclear Materials*, vol. 576, no. 154264, 2023, doi:10.1016/j.jnucmat.2023.154264.
- [27] J.-F. Jue, C. Breckenridge, T. Trowbridge, T. O'Holleran and D. Keiser, "AFIP-6 MKII Characterization Summary Report," *INL/EXT-14-32457 Revision 0, Idaho National Laboratory*, 2014.
- [28] A. Robinson, W. Williams, B. Rabin, J.-F. Jue, D. Keiser and N. Lybeck, "Follow on Investigation of U-Mo Monolithic Fuel Swelling in the AFIP-6 MkII Experiment," *INL/RPT-18-50149 Revision 0, Idaho National Laboratory*, 2018.
- [29] W. Williams, F. Rice, A. Robinson, M. Meyer and B. Rabin, "AFIP-6MII Post-irradiation Examination Summary Report," *INL/EXT-20-34142 Revision 0, Idaho National Laboratory*, 2015.